Acta Pharmaceutica Sinica B 2023;13(11):4523–4534

Chinese Pharmaceutical Association
Institute of Materia Medica, Chinese Academy of Medical Sciences

Acta Pharmaceutica Sinica B

www.elsevier.com/locate/apsb
www.sciencedirect.com

ORIGINAL ARTICLE

The F-box-only protein 44 regulates pregnane X receptor protein level by ubiquitination and degradation

Rebecca R. Florke Gee[a,b], Andrew D. Huber[a], Jing Wu[a], Richa Bajpai[c], Allister J. Loughran[c], Shondra M. Pruett-Miller[c], Taosheng Chen[a,*]

[a]*Department of Chemical Biology and Therapeutics, St. Jude Children's Research Hospital, Memphis, TN 38105, USA*
[b]*Graduate School of Biomedical Sciences, St. Jude Children's Research Hospital, Memphis, TN 38105, USA*
[c]*Center for Advanced Genome Engineering and Department of Cell and Molecular Biology, St. Jude Children's Research Hospital, Memphis, TN 38105, USA*

Received 30 March 2023; received in revised form 24 May 2023; accepted 13 June 2023

KEY WORDS

PXR;
FBXO44;
Ubiquitination;
Proteasomal degradation;
CYP3A4;
Drug–drug interactions;
E3 ligase;
Nuclear receptor

Abstract Pregnane X receptor (PXR) is a ligand-activated nuclear receptor that transcriptionally upregulates drug-metabolizing enzymes [*e.g.*, cytochrome P450 3A4 (CYP3A4)] and transporters. Although the regulation of PXR target genes is well-characterized, less is known about the regulation of PXR protein level. By screening an RNAi library, we identified the F-box-only protein 44 (FBXO44) as a novel E3 ligase for PXR. PXR abundance increases upon knockdown of FBXO44, and, inversely, decreases upon overexpression of FBXO44. Further analysis revealed that FBXO44 interacts with PXR, leading to its ubiquitination and proteasomal degradation, and we determined that the F-box associated domain of FBXO44 and the ligand binding domain of PXR are required for the functional interaction. In summary, FBXO44 regulates PXR protein abundance, which has downstream consequences for *CYP3A4* levels and drug–drug interactions. The results of this study provide new insight into the molecular mechanisms that regulate PXR protein level and activity and suggest the importance of considering how modulating E3 ubiquitin ligase activities will affect PXR-mediated drug metabolism.

*Corresponding author.
E-mail address: taosheng.chen@stjude.org (Taosheng Chen).

Peer review under responsibility of Chinese Pharmaceutical Association and Institute of Materia Medica, Chinese Academy of Medical Sciences.

https://doi.org/10.1016/j.apsb.2023.07.014

1. Introduction

Pregnane X receptor (PXR) is a nuclear receptor that governs the liver detoxification system. Previous studies have established that PXR exhibits ligand promiscuity and may be activated by many diverse compounds, both endogenous and exogenous[1,2]. Upon agonist binding, PXR transcriptionally up-regulates genes encoding drug-metabolizing enzymes, such as the cytochrome P450 (CYP) family of enzymes (*e.g.*, CYP3A4) and transporters (*e.g.*, the efflux pump protein MDR1)[3−5]. Besides drug metabolism, PXR is involved in physiological processes, such as glucose and lipid metabolism and detoxification of bile acids and bilirubin, and has been implicated in diseases like hepatic steatosis, inflammatory bowel disease, diabetes, and various cancers[6−14]. *CYP3A4* is a vital PXR target gene because it is responsible for metabolizing many clinical drugs; thus, pharmaceuticals that activate PXR, such as the antibiotic rifampicin and the antiviral ritonavir, increase the risk of drug resistance, drug−drug interactions, and liver toxicity[15,16]. To avoid these undesirable PXR-mediated effects, pharmaceutical companies expend significant resources to eliminate PXR activation by drug candidates. Consequently, the downstream regulation of the PXR signaling cascade and its target genes is well-characterized, but less is known about the natural modulation of PXR protein level and activity.

Ubiquitination is the process by which ubiquitin is added to lysine residues of target proteins, occurring through an enzyme cascade involving an E1 ubiquitin-activating enzyme, an E2 ubiquitin-conjugating enzyme, and an E3 ubiquitin ligase[17]. Ubiquitination leads to distinct outcomes, depending on the linkage and length of the ubiquitin chain. For example, poly-ubiquitin Lys48 (K48)-linked chains typically signal for proteasomal degradation, while monoubiquitination may alter a protein's interactions, activity, or subcellular localization[17]. Many proteins rely on the ubiquitin−proteasome degradation pathway for turnover and homeostatic regulation[17−21]. Three different E3 ligases (RBCK1, UBR5, and TRIM21) have thus far been reported to interact with PXR[22−24], suggesting that additional E3 ligases may be involved in regulating PXR stability, depending on the cellular or tissue context.

In this study, we performed an siRNA screen to better understand the regulation of PXR by the cellular ubiquitination pathway and identified F-box-only protein 44 (FBXO44) as a candidate E3 ligase for PXR. FBXO44 has been reported to act as the substrate adaptor in two distinct E3 ligase complexes, the SKP1−CUL1−FBXO44 complex[25] and the CUL4B−DDB1−FBXO44 complex[26]. We found that PXR protein amount increases upon knockdown of FBXO44 and decreases with overexpression of FBXO44 and that FBXO44 interacts with and ubiquitinates PXR, regulating PXR protein level through the proteasome pathway. Furthermore, FBXO44 knockdown-mediated increase in PXR protein amount correlated with an increase in *CYP3A4* expression and PXR inducibility by prototypical PXR agonists. The results of this study provide additional insight into the molecular mechanisms that regulate PXR protein level and activity.

2. Materials and methods

2.1. Materials

Lipofectamine 3000 and Lipofectamine RNAiMAX transfection reagents, penicillin−streptomycin and puromycin stock solutions, Opti-MEM reduced serum medium, cycloheximide, and DMSO were all purchased from Thermo Fisher Scientific (Atlanta, GA, USA). Fetal bovine serum (FBS) was purchased from HyClone (Logan, UT, USA). Actinomycin D was purchased from Cell Signaling Technology (Danvers, MA, USA). Rifampicin and MG132 were purchased from MilliporeSigma (Burlington, MA, USA), and dTAG-13 was purchased from MedChemExpress (Monmouth Junction, NJ, USA). Nano-Glo HiBiT Lytic Detection System, CellTiter-Glo Luminescent Cell Viability Assay, and Nano-Glo Live Cell Assay System were purchased from Promega (Madison, WI, USA). All tissue culture supplemental materials, such as tissue culture flasks and disposable pipettes, were purchased from Corning (Corning, NY, USA). All oligonucleotides were from Integrated DNA Technologies (Coralville, IA, USA) and are presented in Supporting Information Table S1.

2.2. Cell culture, plasmids, and cell line generation

SNU-C4 cells were obtained from the Korean Cell Line Bank (KCLB, cat. no. 0000C4) and maintained in RPMI-1640 medium (ATCC) with 10% FBS (HyClone). HepG2/C3A cells were obtained from the American Type Culture Collection (ATCC, cat. no. CRL-10741) and maintained in Eagle's minimum essential medium (EMEM, ATCC) with 10% FBS. 293T cells were obtained from ATCC (cat. no. CRL-3216) and maintained in Dulbecco's modified Eagle's medium (DMEM, ATCC) with 10% FBS. HepaRG 5F parental cells (cat. no. MTOX1010-1VL) were purchased from Sigma−Aldrich (St. Louis, MO, USA) and maintained according to the provider's instructions and as previously described[27]. All cell lines were authenticated by short tandem repeat DNA profiling. Cells were incubated in a humidified atmosphere at 37 °C with 5% CO_2 and routinely verified to be mycoplasma free by using the MycoProbe Mycoplasma Detection Kit (R&D Systems). Cell counts were obtained with a Countess II Automated Cell Counter using trypan blue staining.

To generate the 293T-FLAG-PXR cells, 293T cells were transfected with a pcDNA3-FLAG-PXR plasmid, containing NeoR[28], using Fugene 6 (Promega) following the manufacturer's standard protocol. Forty-eight hours after transfection, cells were selected with 1 mg/mL geneticin (Life Technologies, cat. no. 10131-027). After selecting cells for 2−4 weeks, stable expression of FLAG-PXR protein was confirmed by Western blot. Cells were continuously cultured in the presence of 1 mg/mL geneticin after selection.

SNU-C4 3xFLAG-PXR KI cells were previously generated using CRISPR/Cas9 technology[29]. SNU-C4 HiBiT-PXR KI cells and 293T FBXO44 KO cells were generated using CRISPR-Cas9 technology in the Center for Advanced Genome Engineering (St. Jude). Briefly, 500,000 SNU-C4 or 293T cells were transiently co-transfected with precomplexed ribonuclear proteins consisting of 100 pmol of chemically modified sgRNA (Synthego), 33 pmol of Cas9 protein (St. Jude Protein Production Core), 200 ng of pMaxGFP (Lonza), and if required 3 μg of ssODN donor. The transfections were performed *via* nucleofection (Lonza, 4D-Nucleofector X-unit) using solution P3 and program DS-150 (SNU-C4) or CM-130 (293T) in a small (20 μL) cuvette according to the manufacturer's recommended protocol. Single cells were sorted based on transfected cells (GFP+) five days post-nucleofection into 96-well plates containing prewarmed media and were clonally expanded. Clones were screened and verified for the desired modification using targeted deep sequencing

analyzed with CRIS.py as previously described[30]. Final clones tested negative for mycoplasma by the MycoAlert Plus Mycoplasma Detection Kit (Lonza) and were authenticated using the PowerPlex Fusion System (Promega) performed at the Hartwell Center (St. Jude). Editing construct sequences and screening primers are listed in Table S1.

2.3. Plasmids, siRNAs, and transfections

All plasmids used for transient transfection were in the pcDNA3 vector. FLAG-PXR was previously described[28]. The FLAG-PXR truncation constructs with various deletions were constructed with the Q5 Site-Directed Mutagenesis Kit (New England Biolabs; Ipswich, MA, USA) using FLAG-PXR as a template and the appropriate primer pairs (Table S1). To make the FLAG-eGFP-PXR plasmids, eGFP was amplified from peGFP-C3 (Clontech) and assembled into the FLAG-PXR vector with NEBuilder HiFi DNA Assembly Master Mix (New England Biolabs). The FLAG-eGFP empty vector was subsequently made by removing PXR from FLAG-eGFP-PXR with BamHI digestion followed by circularization with T4 DNA ligase (New England Biolabs). MYC-FBXO44 was purchased from GenScript (Piscataway, NJ) and used as template to construct MYC-FBXO44 ΔF-box and ΔFBA with the Q5 Site-Directed Mutagenesis Kit using P14 and P15 or P16 and P17, respectively. To generate MYC-FKBP^{F36V}-FBXO44, FKBP^{F36V} was amplified from pcDNA3-FKBP^{F36V}-HA-PXR[29] with P18 and P19 and assembled with the MYC-FBXO44 vector using NEBuilder HiFi Assembly Master Mix. LgBiT-Ubiquitin was synthesized by ThermoFisher Scientific. To construct SmBiT-PXR-LBD, SmBiT-PXR was generated first with P20 and P21 using FLAG-PXR as a template; then, SmBiT-PXR was used as a template with P22 and P23 to generate SmBiT-PXR-LBD with the Q5 Site-Directed Mutagenesis Kit.

Cells were reverse transfected with siRNAs at a final concentration of 25 nmol/L using Lipofectamine RNAiMAX and were analyzed after 72 h. The siRNA library (Supporting Information Table S2), non-targeting siRNA (si*NT*; D-001210-05), and siRNAs targeting PXR [si*PXR*; NR1I2 SMARTpool (M-003415-02)] or FBXO44 [si*FBXO44*: FBXO44 SMARTpool (M-019201-01) and individual (D-019201-01, D-019201-02, D-019201-03, and D-019201-04)] were purchased from Horizon Discovery (Lafayette, CO, USA). An additional siRNA targeting *FBXO44* (no. SI00145663) was purchased from Qiagen.

For overexpression, cells were seeded for 24 h at 60% confluence before they were transfected with the appropriate plasmids using Lipofectamine 3000. Unless otherwise noted, cells were harvested 48 h post-transfection.

2.4. HiBiT and NanoBiT assays

For the siRNA screen, SNU-C4 HiBiT-PXR KI cells were reverse transfected with the siRNA library using Lipofectamine RNAiMAX in white tissue culture-treated 384-well plates. An Echo 655T Acoustic Liquid Handler (Beckman Coulter) was used to dispense 300 nL/well of each siRNA at 2.5 μmol/L stock concentration. Lipofectamine RNAiMAX was diluted to 1% in OptiMEM and 10 μL was added to each well. Then, SNU-C4 HiBiT-PXR KI cells were added to the wells (5×10^3 cells/well in 20 μL RPMI-1640 with 10% FBS). The next day, 30 μL of media was added to each well. After incubating the plates for a total of three days, 35 μL of media was aspirated by a BioTek ELx405. Nano-Glo HiBiT Lytic Detection System or CellTiter-Glo Luminescent Cell Viability Assay and an EnVision microplate reader (PerkinElmer) were used to measure HiBiT signal or cell viability, respectively. Results are reported as fold change relative to siNT control cells.

For the NanoBiT assay, 293T FBXO44 KO cells were plated in tissue culture-treated 12-well plates (2×10^5 cells/well in 1 mL DMEM with 10% FBS). The next day, cells were transfected with 100 ng each of SmBiT-PXR LBD, LgBiT-ubiquitin, and MYC-FBXO44, MYC-FBXO44 ΔF-box, or MYC-FBXO44 ΔFBA using Lipofectamine 3000. The pcDNA3 empty vector was added to keep the total DNA amount used in each transfection equal. After 24 h, cells were trypsinized, resuspended in media, and plated in white tissue culture-treated 384-well plates (1.5×10^4 cells/well in 20 μL medium). The next day, cells were treated with 10 μmol/L MG132 (final DMSO concentration = 0.5%) for 4 h. Nano-Glo Live Cell Assay System and an EnVision microplate reader were used to measure the reconstituted NanoBiT signal. Results are reported as fold change relative to cells expressing SmBiT-PXR LBD and LgBiT-ubiquitin.

2.5. Western blotting

Cells were washed with DPBS, trypsinized, pelleted by centrifugation, and lysed in Pierce RIPA buffer (ThermoFisher Scientific) supplemented with Halt Protease Inhibitor Cocktail (Thermo Fisher Scientific). Protein in the lysate was quantified with the Pierce BCA Protein Assay Kit (ThermoFisher Scientific), diluted with NuPAGE LDS Sample Buffer (ThermoFisher Scientific), and heated at 95 °C for 5 min. Then, 20 μg of each sample was loaded into NuPAGE 4%−12% Bis−Tris gels (Thermo Fisher Scientific). Separated proteins were transferred to nitrocellulose membranes using the iBlot 2 Dry Blotting System (ThermoFisher Scientific). Membranes were blocked with TBST [50 mmol/L Tris (pH 7.4), 150 mmol/L NaCl, 0.1% Tween 20] containing 5% milk for 1 h at room temperature. Primary antibodies were used at 1:1000 dilution in TBST containing 5% milk and incubated with the membranes overnight at 4 °C. The following primary antibodies were used: mouse anti-FLAG M2 (Sigma−Aldrich, cat. no. F3165), mouse anti-β-actin (Sigma−Aldrich, cat. no. A5441), rabbit anti-β-actin (Cell Signaling Technology, cat. no. 4967L), mouse anti-MYC-tag 9B11 (Cell Signaling Technology, cat. no. 2276S), rabbit anti-FBXO44 (Sigma−Aldrich, cat. no. HPA003363), mouse anti-PXR H-11 (Santa Cruz Biotechnology, cat. no. sc-48340), and rabbit anti-ubiquitin (Cell Signaling Technology, cat. no. 3933S). Membranes were washed with TBST three times for 10 min each, and IRDye 800CW Goat anti-Mouse IgG Secondary Antibody (LI-COR, cat. # 926-32210, 1:10,000 dilution) and IRDye 680LT Goat anti-Rabbit IgG Secondary Antibody (LI-COR, cat. # 926-68021, 1:10,000 dilution) were added in TBST containing 5% milk for 1 h at room temperature. Membranes were washed as above and imaged with an Odyssey CLx imaging system (LI-COR). Bands were quantified with Image Studio Lite Software (LI-COR). The relative band intensity of the indicated control sample (*e.g.*, empty vector control or 0 h time point) was set as 1 for comparisons with test samples.

2.6. Coimmunoprecipitation assays

293T cells were plated in tissue culture-treated 10 cm plates (3.5×10^6 cells in 10 mL DMEM with 10% FBS) and were transfected the next day using Lipofectamine 3000 with 3 μg of each pcDNA3 construct (6 μg total DNA). Two days after

transfection, cells were washed with DPBS and lysed in Pierce IP lysis buffer (ThermoFisher Scientific, cat. no. 87788) supplemented with Halt Protease Inhibitor Cocktail and PhosSTOP (Roche). Five to ten percent of each sample lysate was kept as input, and equal amounts of the sample lysates were used for coimmunoprecipitation pulldowns. Immunoprecipitation was performed by adding 3 μL of rabbit IgG (Cell Signaling Technology, cat. no. 2729S), anti-FLAG (Sigma−Aldrich, cat. no. F7425), or anti-FBXO44 (Sigma−Aldrich, cat. no. HPA003363) and 50 μL of prepared Dynabeads Protein G (Thermo Fisher Scientific, cat. no. 10003D) to each sample. The samples were incubated overnight at 4 °C with gentle rotation. Bead−antibody−protein complexes were washed four times with PBS, and samples were eluted in 1 × NuPage sample buffer with reducing agent and heated for 5 min at 95 °C. The eluted samples were subsequently analyzed by Western blot with mouse anti-FLAG M2, mouse anti-β-actin, and mouse anti-MYC-tag 9B11 antibodies, as described above.

2.7. *RNA isolation and quantitative real-time polymerase chain reaction analysis (RT-qPCR)*

Total RNA was isolated from cells with Maxwell 16 LEV simplyRNA Tissue Kits (Promega). cDNA was generated from 2 μg of RNA by using the SuperScript VILO cDNA Synthesis Kit (ThermoFisher Scientific). 2 μL of cDNA was used to perform quantitative RT-PCR, using TaqMan Fast Advanced Master Mix (Applied Biosystems) and TaqMan gene expression assays specific for *PXR* (Hs01114267_m1) and *CYP3A4* (Hs00604506_m1) (ThermoFisher Scientific). 18S rRNA (Hs03928990_g1) was used as the reference gene, and qPCR was performed using the 7500 Fast Real-Time PCR System (Applied Biosystems, Waltham, MA, USA). Fold induction values were calculated according to Eq. (1):

$$\text{Fold change} = 2^{-\Delta\Delta Ct} \quad (1)$$

where ΔCt represents the differences in cycle threshold numbers between the target gene and the reference gene and ΔΔCt represents the relative change in these differences between the control and treatment groups[31].

2.8. *Plotting and statistical analyses*

All plots were made in GraphPad Prism 9. Results are expressed as the mean ± standard deviation from at least three independent experiments. Significance was assessed with Student's *t*-test to compare the means of two groups, one-way ANOVA followed by Dunnett's multiple comparisons test for all samples compared to the control, or two-way ANOVA followed by Šidák's multiple comparison test [$P \leq 0.05$ (*), $P \leq 0.01$ (**), $P \leq 0.001$ (***), $P \geq 0.05$ (non-significant, ns)].

3. Results

3.1. *siRNA screen identifies E3 ligase(s) that regulate(s) PXR protein level*

To identify E3 ligase(s) responsible for regulating PXR protein abundance, we first required a high-throughput assay to detect changes in PXR protein level. HiBiT tagging is a simple, sensitive bioluminescent method for quantifying protein abundance, even endogenous proteins expressed at low levels, making it well-suited for detecting changes in PXR protein level in a high-throughput manner[32,33]. We chose the colorectal SNU-C4 cell line because it is among cell lines with the highest *PXR* mRNA levels[29,34,35], and the PXR protein in this cell line is activated by PXR agonists and blocked by a PXR antagonist[34]. In addition, we previously developed a knock in cell model that contains a 3xFLAG tag in the N-terminus of PXR (SNU-C4 3xFLAG-PXR KI)[29], indicating the feasibility of tagging PXR with HiBiT to measure endogenous PXR protein level for this study. Indeed, we successfully used CRISPR/Cas9 to knock in a HiBiT tag to the N-terminus of PXR (referred to as SNU-C4 HiBiT-PXR KI cells) (Supporting Information Fig. S1A). We confirmed the presence of the HiBiT tag on PXR by sequencing and by showing that the HiBiT-dependent luminescence signal decreased upon siRNA-mediated knockdown of PXR (Fig. S1B).

We screened a custom siRNA library targeting 839 proteins that are components of the ubiquitination-proteasome pathway, including the ubiquitin genes, E2 ubiquitin-conjugating enzymes, and E3 ubiquitin ligases (Table S2). For the screen, we transfected SNU-C4 HiBiT-PXR KI cells with the siRNA library for three days and then measured HiBiT-dependent luminescence as an indicator of endogenous PXR protein level (Fig. 1A). The screening results were normalized to non-targeting siRNA (siNT) to calculate fold change (FC) in HiBiT-PXR protein amount (Fig. 1B). Treatment with the proteasome inhibitor MG132 was also included as a positive control, which increased PXR protein level by 1.6-fold (Fig. 1C and Fig. S1C), representing the maximum FC we can likely achieve from the assay. Notably, the proteasomal protein PSMA3 was the top screening hit (Fig. 1C), serving as an internal assay control. The hits were retested in a HiBiT assay with a concomitant CellTiter-Glo viability assay to determine which siRNA targets reproducibly increased PXR protein level without exhibiting significant cytotoxicity upon knockdown (Fig. 1D). Other than PSMA3, FBXO44 knockdown resulted in the highest increase of HiBiT-PXR signal (Fig. 1D), so FBXO44 was selected for further investigation.

3.2. *FBXO44 regulates PXR protein level*

To visualize the change in PXR protein level by Western blot, we used the previously developed SNU-C4 3xFLAG-PXR KI cells[29]. PXR protein significantly increased upon FBXO44 knockdown in SNU-C4 3xFLAG-PXR KI cells, and we confirmed the siRNA-mediated knockdown of FBXO44 by Western blot (Fig. 2A). We obtained similar results with FBXO44 knockdown in 293T cells stably expressing CMV-driven FLAG-PXR (293T-FLAG-PXR) (Fig. 2B). Both pooled and individual siRNAs were tested for their effects on increasing PXR protein amount, and we chose the individual siRNA #4 for additional experiments (Fig. 2C and Supporting Information Fig. S2). In addition, we tested another siRNA (Q1) that was previously reported to target the 3′ UTR of *FBXO44*[36], and we observed a similar increase in PXR protein (Fig. 2D). Conversely, and consistent with our hypothesis that FBXO44 acts as an E3 for PXR, overexpression of FBXO44 decreased endogenous PXR protein abundance (Fig. 2C).

Unexpectedly, in addition to increasing PXR protein level, siFBXO44 also increased *PXR* mRNA (Fig. 3A). This was observed in both SNU-C4 3xFLAG-PXR KI and 293T-FLAG-PXR cells (Fig. 3A), indicating this effect was not due to FBXO44 affecting the endogenous *PXR* promoter. To determine whether

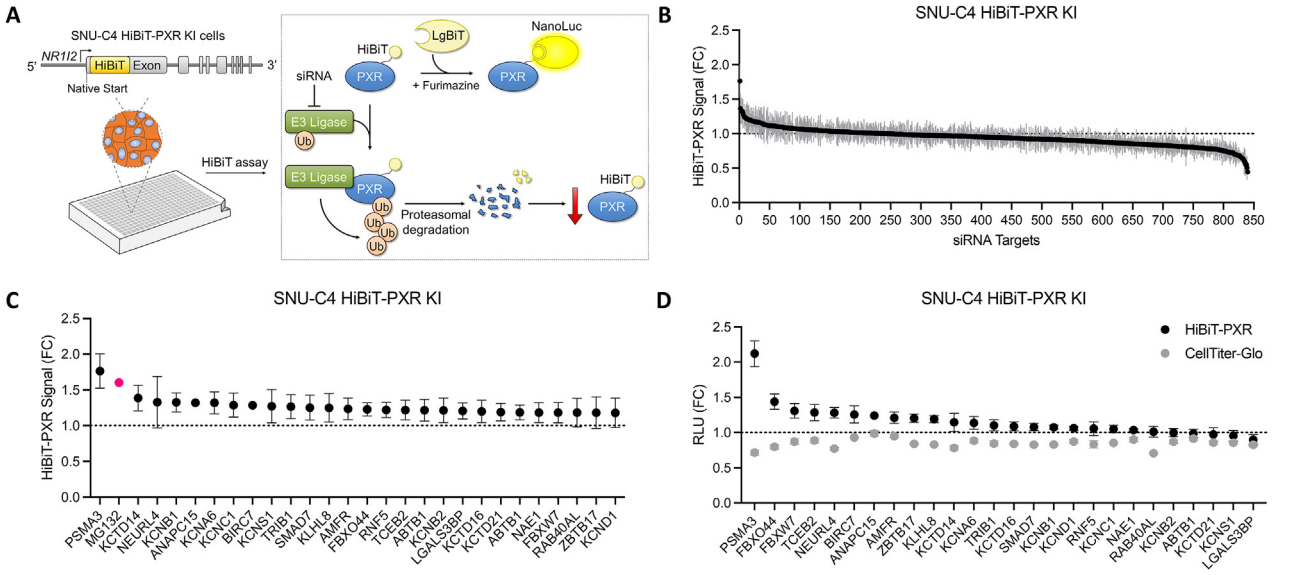

Figure 1 siRNA screen to identify E3 ligase(s) for PXR. (A) Schematic of the HiBiT-PXR RNAi screen to identify potential E3 ligases. (B) RNAi screening results, where HiBiT-PXR signal was measured 3 days after transfection with siRNA. Fold change (FC) values were calculated by normalizing to the siNT control. (C) The top screening hits from (B) are shown. The HiBiT-PXR FC after 6 h treatment with 10 μmol/L MG132 is shown as a pink dot. (D) The top hits were re-tested by HiBiT assay and CellTiter-Glo viability assay. Results are expressed as the mean ± standard deviation (SD); $n = 3$.

siFBXO44 increased PXR protein level by increasing its mRNA expression, we treated cells with the transcription inhibitor actinomycin D after FBXO44 knockdown. As shown in Fig. 3B, actinomycin D treatment eliminated the siFBXO44-mediated increase in *PXR* mRNA, while the PXR protein level remained 1.8-fold higher than the non-targeting siRNA control. These data indicate that knockdown of FBXO44 directly increases PXR protein level, independently of its effect on *PXR* mRNA level.

To determine if the observed siFBXO44 effect on PXR protein level occurred during PXR translation, we quantified PXR protein level in the presence of the translation inhibitor cycloheximide after siRNA knockdown of FBXO44 (Fig. 3C). PXR protein was

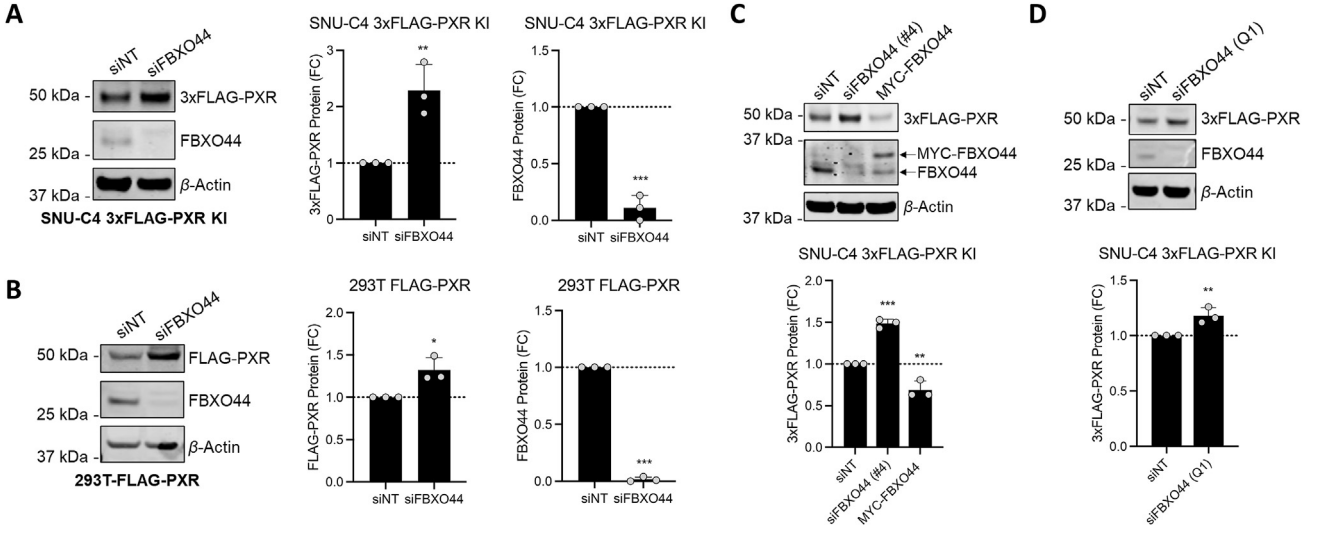

Figure 2 FBXO44 knockdown increases PXR protein level. (A) SNU-C4 3xFLAG-PXR KI or (B) 293T-FLAG-PXR cells were transfected with siNT or siFBXO44 and analyzed by Western blot after 3 days. (C) SNU-C4 3xFLAG-PXR KI cells were transfected with siNT or siFBXO44 (#4). The next day, the cells were transfected with empty vector (pCDNA3) or MYC-FBXO44 for two days and then analyzed by Western blot. (D) SNU-C4 3xFLAG-PXR KI cells were transfected with siNT or siFBXO44 (Q1) and then analyzed by Western blot after 3 days. Graphs show the PXR and FBXO44 protein levels (mean ± SD; $n = 3$), quantified from blots. FC values were calculated by normalizing to the siNT control. Significance was assessed with student's *t*-test (A, B, D) or one-way ANOVA followed by Dunnett's multiple comparisons test for samples compared to the siNT control (C) [$P \leq 0.05$ (*), $P \leq 0.01$ (**), $P \leq 0.001$ (***)].

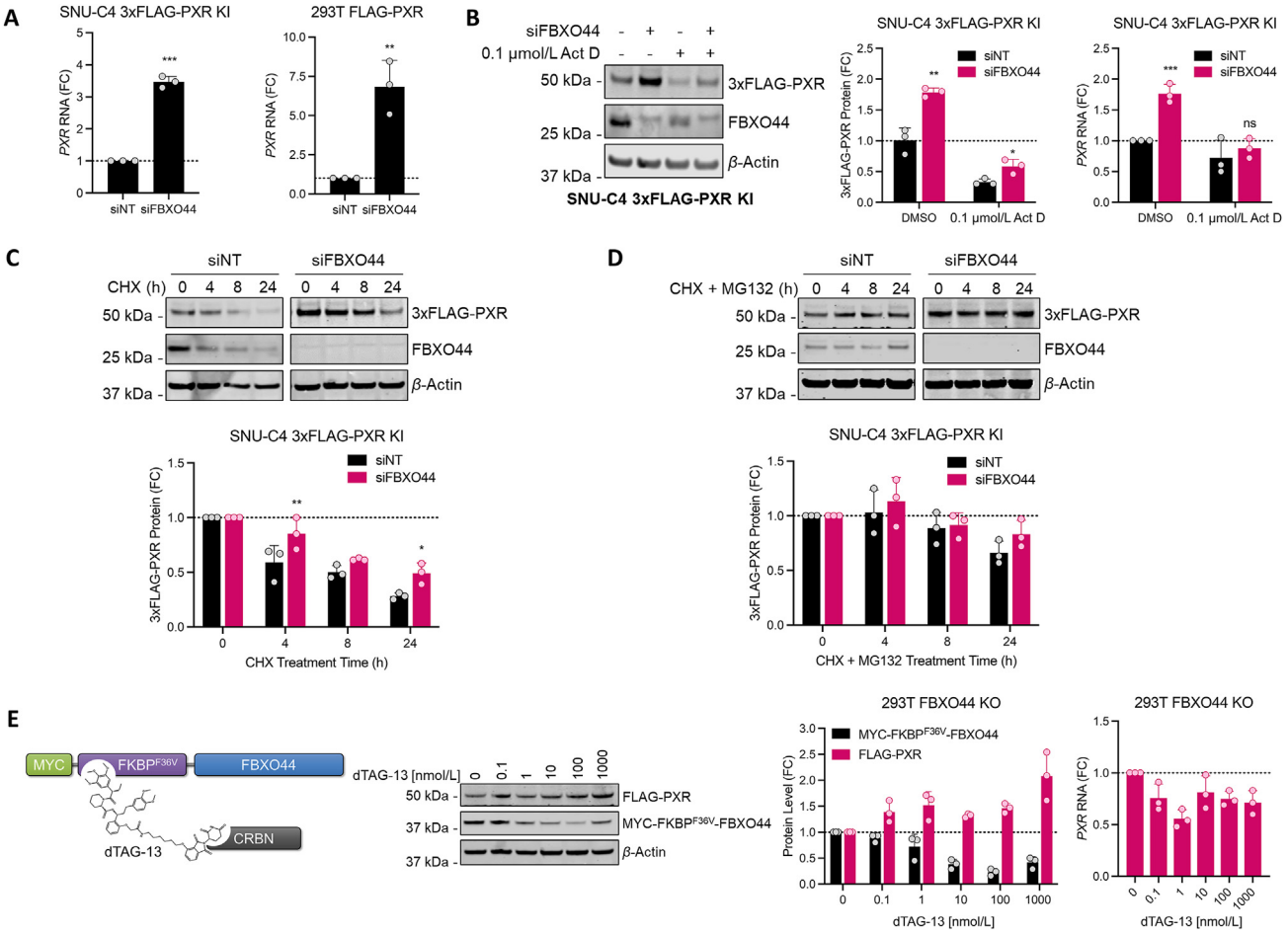

Figure 3 FBXO44 regulates PXR protein level. (A) SNU-C4 3xFLAG-PXR KI or 293T-FLAG-PXR cells were transfected with siNT or siFBXO44 for three days, and *PXR* RNA was measured by RT-qPCR. FC values were calculated by normalizing to 18S RNA and the siNT control. (B) SNU-C4 3xFLAG-PXR KI cells were transfected with siNT or siFBXO44 for 48 h, treated with DMSO or 0.1 μmol/L actinomycin D (Act D) for 24 h, and analyzed by Western blot or RT-qPCR. FC values were calculated by normalizing to the siNT and DMSO-treated control. (C, D) SNU-C4 3xFLAG-PXR KI cells were transfected with siNT or siFBXO44 for three days and then treated with (C) 100 μg/mL cycloheximide (CHX) alone or (D) CHX in combination with 10 μmol/L MG132 for the indicated times. FC values were calculated by normalizing to the DMSO-treated control for either the siNT or siFBXO44 transfected sample group. (E) 293T FBXO44 KO cells were transfected with FLAG-PXR and MYC-FKBP^{F36V}-FBXO44 for 48 h, treated with the indicated doses of dTAG-13 for 24 h, and analyzed by Western blot or RT-qPCR. FC values were calculated by normalizing to the DMSO-treated control for either PXR or FBXO44. Results are expressed as the mean ± SD; $n = 3$. Significance was assessed with student's *t*-test (A, B) or two-way ANOVA followed by Šidák's multiple comparison test (C, D) [$P \leq 0.05$ (*), $P \leq 0.01$ (**), $P \leq 0.001$ (***), $P \geq 0.05$ (non-significant, ns)].

lost at a decreased rate when FBXO44 was depleted in the presence of cycloheximide, and co-treatment with MG132 abolished this difference (Fig. 3C and D), indicating that FBXO44 directly controls PXR protein stability rather than translation.

Because we used siRNA to modulate FBXO44 protein amount, experiments had to be conducted over a period of days to achieve efficient knockdown followed by secondary events (*i.e.*, PXR protein changes). To assess effects on a shorter time scale and further validate that FBXO44 directly affects PXR protein stability, we utilized the degradation tag (dTAG) system[37]. First, we generated FBXO44 knockout (KO) 293T cells by CRISPR/Cas9 (293T FBXO44 KO cells). Next, we created an expression construct with FKBP^{F36V}-tagged FBXO44 to selectively degrade FBXO44 upon treatment with dTAG-13 (Fig. 3E). We then overexpressed FLAG-PXR and MYC-FKBP^{F36V}-FBXO44 in 293T FBXO44 KO cells for 48 h, treated with DMSO or dTAG-13 for 24 h, and assessed PXR and FBXO44 protein levels by Western blot. FBXO44 and PXR exhibited a dose-responsive inverse correlation, as PXR protein levels increased while FBXO44 protein levels decreased (Fig. 3E). We also confirmed that this increase in PXR protein was not due to *PXR* mRNA increase (Fig. 3E, right graph). Taken together, these data suggest that FBXO44 directly regulates PXR protein stability.

3.3. *FBXO44 depletion leads to increased PXR activity*

We next determined whether the siFBXO44-mediated increase in PXR protein level would affect the transcriptional transactivation activity of PXR, using *CYP3A4* RNA expression as an indicator of PXR activity. Treating either SNU-C4 3xFLAG-PXR KI or parental SNU-C4 cells with 10 μmol/L of the PXR agonist rifampicin increased *CYP3A4* expression by 2- to 4-fold,

respectively, in siNT-transfected control cells (Fig. 4A and Supporting Information Fig. S3). The siFBXO44-transfected cells showed an increase in basal PXR activity (DMSO treatment) and a 10-fold increase in *CYP3A4* expression upon rifampicin treatment (Fig. 4A and Fig. S3).

To determine whether FBXO44 affects PXR activity in liver cell models, we knocked down FBXO44 in the commonly studied HepG2 and HepaRG cells. In HepG2, compared to their respective DMSO-treated controls, rifampicin treatment in siNT-transfected cells increased *CYP3A4* by 7-fold, while FBXO44 knockdown increased *CYP3A4* by 14-fold (Fig. 4B). Likewise, HepaRG cells treated with rifampicin after FBXO44 knockdown exhibited a significant increase in *CYP3A4* expression compared to cells transfected with siNT (Fig. 4C).

3.4. *FBXO44 interacts with PXR*

We hypothesized that FBXO44 affects PXR protein abundance by directly interacting with PXR. To test this, we performed coimmunoprecipitation experiments using 293T cells transfected with combinations of empty vector, FLAG-PXR, and MYC-FBXO44. PXR immunoprecipitated with the FLAG antibody as expected, and FBXO44 coimmunoprecipitated only when PXR was present, indicating that the two proteins interact (Fig. 5A).

We next evaluated which PXR regions are necessary for the interaction by using PXR truncation constructs (Fig. 5B). FLAG-tagged PXR mutants were transfected in 293T cells, with all showing high expression, except the DBD, C-LBD, and ΔN mutants that expressed at lower levels. Regardless, all FLAG-PXR variants immunoprecipitated with the FLAG antibody (Fig. 5C). MYC-FBXO44 coimmunoprecipitated with full-length PXR, as well as the Hinge + LBD, LBD, and ΔAF2 mutants (Fig. 5C). In the FBXO44 immunoprecipitation (IP), we observed pulldown of full-length, LBD, Hinge + LBD, ΔN, and ΔAF2 PXR variants. Since PXR C-LBD could not be visually detected in the FBXO44 IP due to obstruction from the light chain of the antibody used for IP, we fused eGFP to selected PXR constructs and again immunoprecipitated with FLAG or FBXO44 antibodies (Fig. 5D). All FLAG-eGFP-PXR constructs were detected in the FLAG and FBXO44 IP samples, but FBXO44 was not detected in the FLAG IP with PXR ΔC (Fig. 5D). The detection of interaction between two proteins might be influenced by how one protein is immunoprecipitated (*e.g.*, FBXO44 IP *vs.* FLAG IP) and how the protein is tagged (*e.g.*, FLAG-PXR *vs.* FLAG-eGFP-PXR). Although we could not precisely map the PXR domain that interacts with FBXO44, our data indicate that FBXO44 interacts with a region of the LBD, but not the DBD of PXR.

Next, to determine if PXR-FBXO44 interaction correlates with decreased PXR protein level, we transfected PXR truncation mutants with empty vector or MYC-FBXO44 in 293T FBXO44 KO cells and performed western blots for total PXR protein (Fig. 5E). In comparison to the respective empty vector controls, FBXO44 expression decreased the protein levels of full-length PXR, Hinge + LBD, and C-LBD mutants, but not DBD and ΔC mutants (Fig. 5E). These results further suggest that both PXR-FBXO44 interaction and FBXO44-dependent PXR protein loss require a region of the PXR LBD.

FBXO44 contains two domains, the F-box domain and the F-box associated (FBA) domain. The F-box domain interacts with SKP1 to form the SKP1-CUL1-F-box-protein-type ubiquitin ligase complex, where the F-box protein dictates the substrate specificity[25,38], and the FBA domain is responsible for interacting with substrates[39]. To identify which FBXO44 domain interacts with PXR, we generated two FBXO44 truncation constructs (Fig. 5F). The full-length FBXO44 and ΔF-box mutant, but not the ΔFBA mutant, coimmunoprecipitated with FLAG-PXR (Fig. 5F). Thus, the FBA of FBXO44 is required for its interaction with PXR, consistent with previous literature identifying the FBA as the substrate-interacting domain[26].

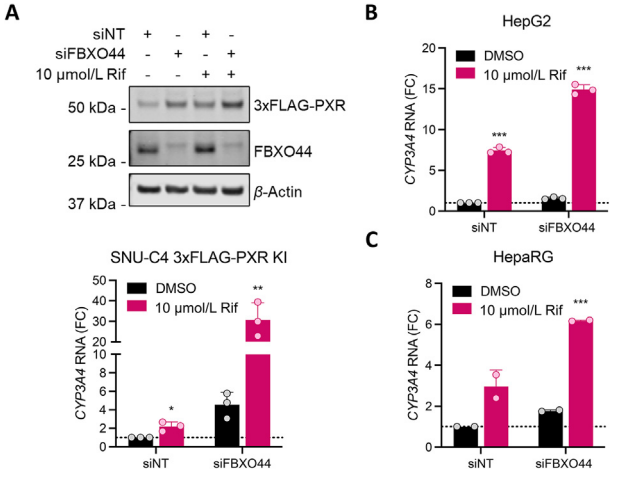

Figure 4 FBXO44 depletion leads to increased PXR activity. (A) SNU-C4 3xFLAG-PXR KI, (B) HepG2, or (C) HepaRG cells were transfected with siNT or si*FBXO44* for two days and then treated with 10 μmol/L rifampicin (Rif) for an additional 24 h. Western blot confirmed the increase in 3xFLAG-PXR protein and the decrease in FBXO44 protein upon FBXO44 KD in SNU-C4 3xFLAG-PXR KI. *CYP3A4* expression was measured by RT-qPCR and normalized to siNT cells treated with DMSO, using 18S RNA as a normalization control. Results are expressed as the mean ± SD; $n = 3$. Significance was assessed with student's *t*-test [$P \leq 0.05$ (*), $P \leq 0.01$ (**), $P \leq 0.001$ (***)].

3.5. *FBXO44 acts as an E3 ubiquitin ligase for PXR*

Consistent with our expectation that FBXO44 regulates PXR protein abundance by acting as an E3 ligase, we observed decreases in both endogenous and overexpressed PXR protein abundance upon overexpression of FBXO44 (Figs. 2C, 5A and 5E, and 6A) and that the FBXO44 FBA domain interacts with PXR (Fig. 5F). To determine whether FBXO44 facilitates ubiquitination of PXR, we designed a NanoBiT-based method to detect PXR ubiquitination by tagging ubiquitin with LgBiT and PXR LBD with SmBiT (Fig. 6B)[32]. In this system, luminescence would be increased when LgBiT-ubiquitin and SmBiT-PXR LBD are in close proximity. If FBXO44 serves as an E3 ligase for PXR, then its expression in 293T FBXO44 KO cells would increase PXR interaction with ubiquitin, leading to higher luminescence from the reconstituted NanoBiT. Indeed, we found that the introduction of FBXO44, but not the ΔF-box or ΔFBA mutant, increased the NanoBiT luminescence (Fig. 6B).

Next, we assessed the natural polyubiquitination of PXR. We inhibited proteasomal degradation in 293T cells transfected with FLAG-PXR and empty vector or MYC-FBXO44 by treating the cells with 10 μmol/L MG132 for 4 h (Fig. 6C). By Western blot, we observed more high-molecular-weight smearing above FLAG-

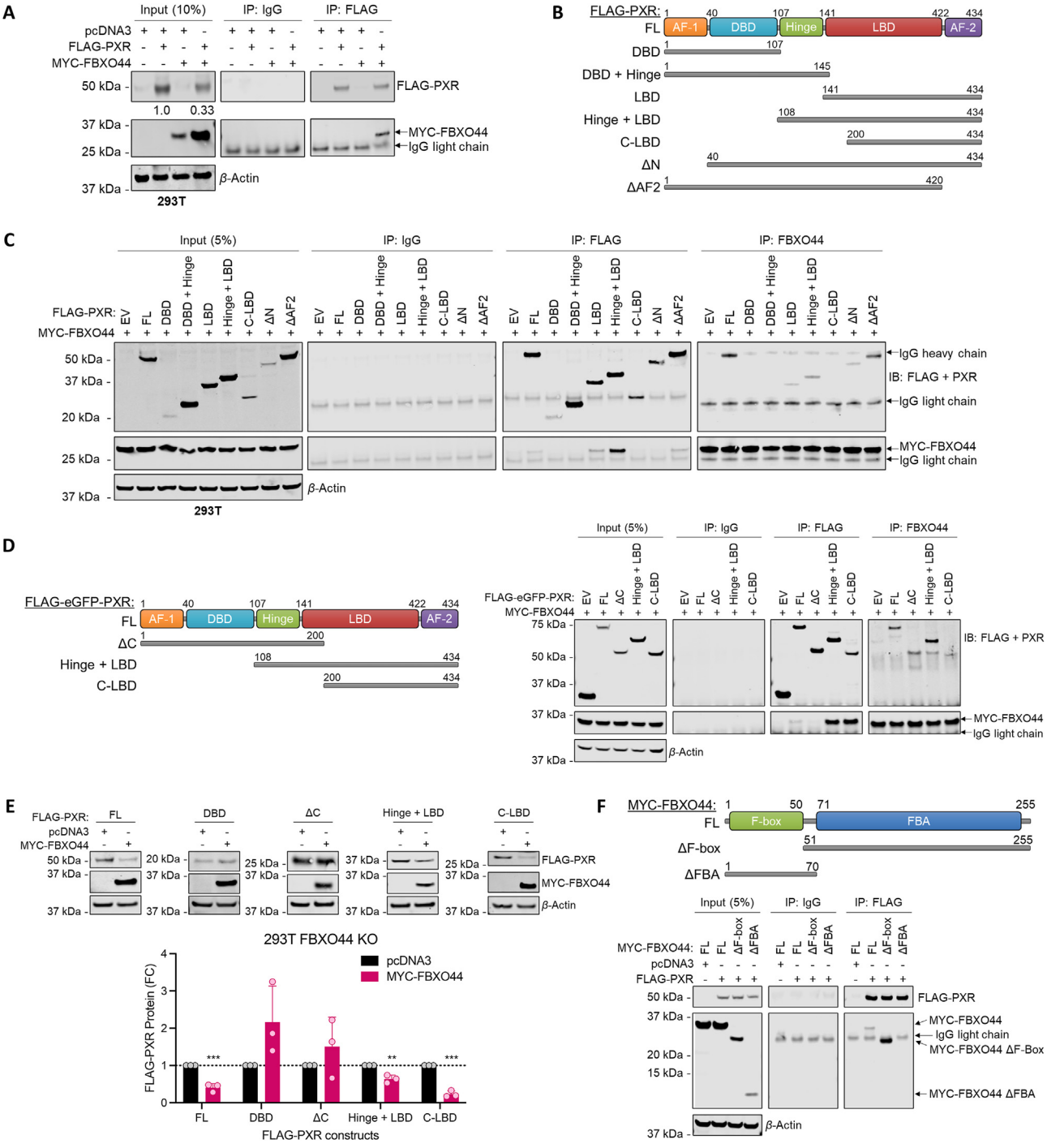

Figure 5 The FBA domain of FBXO44 interacts with the LBD of PXR. (A) 293T cells were transfected with the indicated constructs for 48 h before lysis and immunoprecipitation with rabbit IgG or FLAG antibodies. (B, C) FLAG-PXR or (D) FLAG-eGFP-PXR truncation constructs were overexpressed in 293T cells and used for IP with rabbit IgG, FLAG, or FBXO44 antibodies. (E) The indicated FLAG-PXR truncation constructs were expressed with pcDNA3 empty vector or MYC-FBXO44, and the FLAG-PXR protein level was quantified by Western blot. The graph shows the FLAG-PXR protein amount relative to the empty vector control for each construct (mean ± SD; $n = 3$). Significance was assessed with student's *t*-test [$P \leq 0.01$ (**), $P \leq 0.001$ (***)]. (F) FBXO44 truncation constructs were transfected in 293T FBXO44 KO cells and used for IP with rabbit IgG or FLAG antibodies. Mouse antibodies to FLAG, MYC, and β-actin were used to probe the blots.

PXR when FBXO44 was present (Fig. 6C, top panel), indicative of increased PXR polyubiquitination. These results provide further evidence that FBXO44 serves as an E3 ubiquitin ligase for PXR.

4. Discussion

PXR-mediated elevation of *CYP3A4* expression has been linked to the cross-reactivity of drugs, increasing the risk for drug−drug

interactions[16]. Thus, understanding the regulation of PXR protein by the ubiquitination pathway may shed light on how to prevent inappropriate PXR activity. In the present study, we identified FBXO44 as a candidate E3 ligase for PXR from an siRNA screen. Upon knockdown of FBXO44, PXR protein level increased, which led to an increase in *CYP3A4* expression when cells were treated with the PXR agonist rifampicin. Therefore, modulating a PXR-targeting E3 ubiquitin ligase may affect drug metabolism pathways by altering abundance of the xenobiotic sensor PXR.

Besides its role in xenobiotic drug metabolism, PXR also regulates additional processes of liver physiology, including energy metabolism and detoxification of endobiotics. We observed an increase in *CYP3A4* expression in DMSO-treated cells transfected with siFBXO44 (Fig. 4A and C, and Supporting Information Fig. S3), suggesting that increased PXR protein level leads to increased basal transcriptional activity. Further studies are needed to determine whether other PXR target genes (*e.g.*, *CYP27A1*, *ABCC2*, *UGT1A1*, and *OATP2*) are also upregulated upon siFBXO44-mediated increase in PXR protein abundance, as this result would have broader implications in cholesterol metabolism and detoxification of bile acids and bilirubin[40–44]. PXR is also involved in regulating gluconeogenesis and lipid homeostasis in the liver, mainly through cross-talk with transcription factors, so future investigations could determine whether the siFBXO44-mediated increase in PXR protein level potentiates PXR's suppression of gluconeogenesis and induction of lipogenesis[11,45].

Although three other E3 ligases have been reported for PXR (RBCK1, UBR5, and TRIM21)[22–24], we did not identify them as hits in our three-day siRNA screen. Only UBR5 knockdown was able to increase PXR protein in a screen with extended siRNA incubation time (Supporting Information Fig. S4). Since none of the previous studies used SNU-C4 cells, it is conceivable that different E3 ligases may be involved in PXR protein homeostasis in different cellular environments or tissues. PXR is abundantly expressed in the liver, small intestine, and colon[15], but PXR has also been detected in the breast, stomach, adrenal gland, bone marrow, specific regions of the brain, and at the blood-brain barrier (Supporting Information Fig. S5A)[46–49]. In contrast, FBXO44 is ubiquitously expressed with the highest levels observed in the brain and kidney and the lowest levels in the heart and liver (Fig. S5B)[50,51]. Comparatively, FBXO44 expression is at its lowest in the liver, which may contribute to the high level of PXR protein in the liver[52]. However, a true correlation between their protein levels cannot be made in the absence of PXR proteomics data. One could also speculate that different E3 ligases may mediate PXR degradation depending on the ligand bound to PXR or its subcellular localization. Indeed, ligands are known to drastically alter PXR conformation, which could, in turn, alter E3 recognition[53]. Additional studies are needed to understand how subcellular localization impacts FBXO44-mediated degradation of PXR.

Of the 69 F-box family members, FBXO44 is one of the least characterized proteins[54,55]. FBXO44 belongs to an F-box protein subfamily of FBA domain-containing proteins, where all except FBXO44 bind to glycosylated substrates[39,50]. FBXO44 has only two reported substrates for ubiquitination, BRCA1 and RGS2[25,26], with PXR now being the third. Interestingly, FBXO44 is only capable of

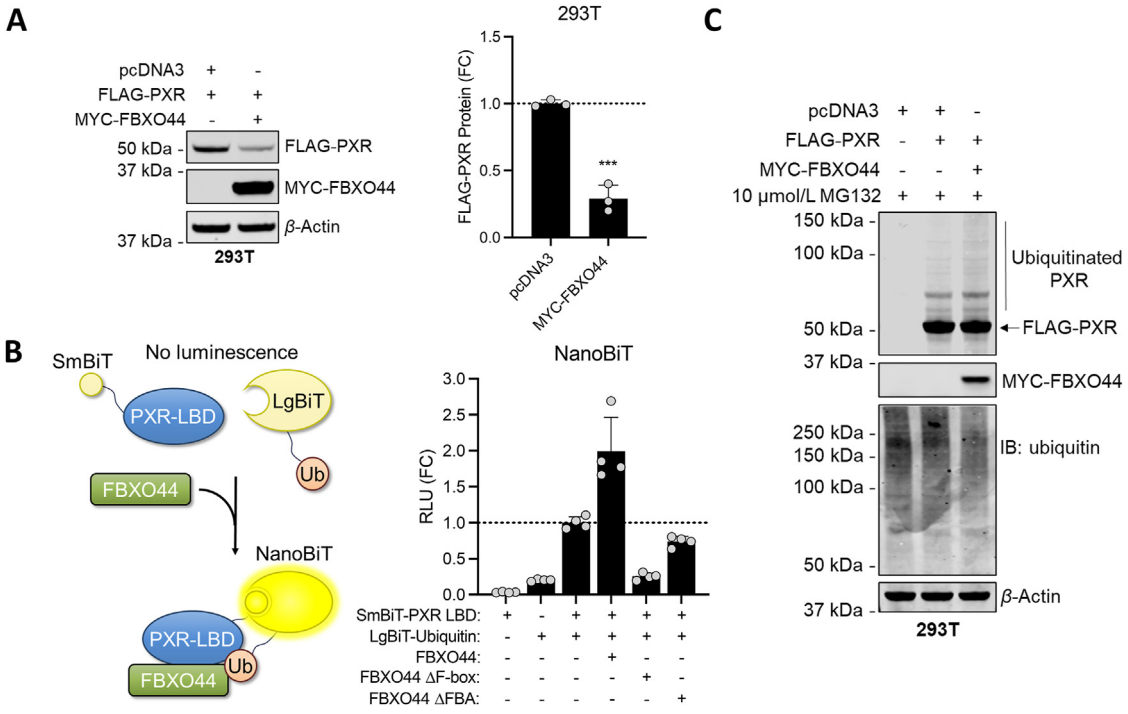

Figure 6 FBXO44 mediates PXR degradation through ubiquitination. (A) 293T cells were transfected with FLAG-PXR and empty vector (pCDNA3) or MYC-FBXO44 for 48 h. FLAG-PXR protein abundance is plotted as FC compared to the empty vector control (mean ± SD; $n = 3$). Significance was assessed with student's *t*-test [$P \leq 0.001$ (***)]. (B) Schematic of NanoBiT-based method for detecting PXR ubiquitination, where ubiquitin is tagged with LgBiT and PXR LBD with SmBiT. 293T FBXO44 KO cells were transfected with the indicated plasmids for 48 h and treated with 10 μmol/L MG132 for 4 h before the NanoBiT assay. FC values were calculated relative to the samples co-transfected with SmBiT-PXR LBD and LgBiT-Ubiquitin (mean ± SD; $n = 4$). (C) 293T cells were transfected with FLAG-PXR and empty vector (pCDNA3) or MYC-FBXO44 for 48 h, treated with 10 μmol/L MG132 for 4 h, and analyzed by Western blot. Anti-PXR (H-11) antibody was used to detect PXR and the high-molecular-weight smearing, indicative of ubiquitination.

mediating the ubiquitination and degradation of RGS2 when in complex with CUL4B-DDB1 and not CUL1-SKP1[26]. Further biochemical studies are needed to determine whether one of these complexes or a new complex is involved in the FBXO44-mediated degradation of PXR. It also remains to be studied whether phosphorylation plays a role in FBXO44 recognition of PXR, as many F-box proteins recognize phospho-degrons in their substrates[55].

Little is known about the physiological functions and diseases impacted by FBXO44. Single nucleotide polymorphisms in *FBXO44* were identified in a Spanish population with aggressive periodontitis, but the association was not statistically significant[56]. Copy-number variants in a region of chromosome 1 containing *FBXO44* and seven other genes were discovered in a Chinese family with a type of focal facial dermal dysplasia[57]. A bioinformatics analysis named FBXO44 as a candidate target for the diagnosis and treatment of atherosclerosis[58]. FBXO44 was recently labeled as a subtype signature protein of adenocarcinoma of the esophagogastric junction, where it promoted tumor progression and metastasis[59]. The mechanistic role of FBXO44 in these disparate diseases remains to be uncovered. It is unclear whether changes in *FBXO44* expression contribute to pathophysiological processes or if FBXO44's function as an E3 ligase adaptor protein leads to the ubiquitination of key pathological proteins. PXR activation has been implicated in the development of atherosclerosis[60–63], and increased *PXR* mRNA expression is present in several esophagogastric adenocarcinoma cell lines[35]; however, further investigation is needed to determine whether FBXO44 regulation of PXR protein is involved in these diseases.

Recently, FBXO44 was reported to promote the repression of DNA repetitive elements in cancer cells by recruiting chromatin modifiers, such as the Mi-2/NURD complex and the H3K9me3 (trimethylation of histone H3 lysine 9) methyltransferase SUV39H1[36]. FBXO44 knockdown in cancer cell lines reactivated repetitive elements, leading to DNA replication stress, decreased viability, proliferation, and tumor growth; in addition, FBXO44 knockdown *in vivo* enhanced immunogenicity and immune checkpoint blockade therapy response[36]. The authors concluded that FBXO44 inhibition might be a promising anti-cancer treatment strategy. However, our newly discovered relationship between FBXO44 and PXR/*CYP3A4* suggests the importance of considering how inhibiting FBXO44 will affect PXR-mediated drug metabolism, especially since previous studies have reported that PXR contributes to chemotherapy resistance in several cancers[8,9,64,65].

5. Conclusions

This work 1) describes the development of a HiBiT-PXR KI cell model to measure changes in endogenous PXR protein level when transfected with a siRNA library, which 2) enabled us to identify FBXO44 as an E3 ligase for PXR. Decreased FBXO44 protein level led to increased PXR protein level, which also increased PXR transcriptional activity (*i.e.*, increased levels of *CYP3A4*). FBXO44 and PXR directly interact, with the FBA domain of FBXO44 and PXR LBD facilitating the interaction. FBXO44 regulates PXR protein level by ubiquitination, leading to proteasomal degradation.

Acknowledgments

The graphical abstract was created with BioRender.com. The Hartwell Center at St. Jude Children's Research Hospital performed all DNA sequencing. We thank ALSAC for support, Dr. Joseph T. Opferman, Dr. John D. Schuetz, and members of the Chen laboratory for valuable discussions, and members of the High Throughput Bioscience Center (Duane G. Currier and Dr. Jonathan A. Low) for instrumentation support. Research reported in this publication was supported by the National Institutes of Health National Institute of General Medical Sciences [Grant R35GM118041]. This study was also supported in part by the National Cancer Institute of the National Institutes of Health under Award Number P30 CA021765. The content is solely the responsibility of the authors and does not necessarily represent the official views of the National Institutes of Health.

Author contributions

Rebecca Florke Gee, Andrew Huber, and Taosheng Chen conceived and designed the research; Rebecca Florke Gee conducted experiments and analyzed data. Rebecca Florke Gee, Andrew Huber, and Taosheng Chen wrote the manuscript. Andrew Huber, Jing Wu, Richa Bajpai, Allister Loughran, and Shondra Pruett-Miller developed reagents for this study. All authors have approved the final manuscript.

Conflicts of interest

The authors declare no conflicts of interest.

Appendix A. Supporting information

Supporting data to this article can be found online at https://doi.org/10.1016/j.apsb.2023.07.014.

References

1. Kliewer SA, Goodwin B, Willson TM. The nuclear pregnane X receptor: a key regulator of xenobiotic metabolism. *Endocr Rev* 2002;**23**:687–702.
2. Kliewer SA, Willson TM. Regulation of xenobiotic and bile acid metabolism by the nuclear pregnane X receptor. *J Lipid Res* 2002;**43**:359–64.
3. Bertilsson G, Heidrich J, Svensson K, Asman M, Jendeberg L, Sydow-Backman M, et al. Identification of a human nuclear receptor defines a new signaling pathway for CYP3A induction. *Proc Natl Acad Sci U S A* 1998;**95**:12208–13.
4. Kliewer SA, Moore JT, Wade L, Staudinger JL, Watson MA, Jones SA, et al. An orphan nuclear receptor activated by pregnanes defines a novel steroid signaling pathway. *Cell* 1998;**92**:73–82.
5. Synold TW, Dussault I, Forman BM. The orphan nuclear receptor SXR coordinately regulates drug metabolism and efflux. *Nat Med* 2001;**7**:584–90.
6. Hakkola J, Rysa J, Hukkanen J. Regulation of hepatic energy metabolism by the nuclear receptor PXR. *Biochim Biophys Acta* 2016;**1859**:1072–82.
7. Robbins D, Chen T. Tissue-specific regulation of pregnane X receptor in cancer development and therapy. *Cell Biosci* 2014;**4**:17.
8. Gupta D, Venkatesh M, Wang H, Kim S, Sinz M, Goldberg GL, et al. Expanding the roles for pregnane X receptor in cancer: proliferation and drug resistance in ovarian cancer. *Clin Cancer Res* 2008;**14**:5332–40.
9. Noll EM, Eisen C, Stenzinger A, Espinet E, Muckenhuber A, Klein C, et al. CYP3A5 mediates basal and acquired therapy resistance in different subtypes of pancreatic ductal adenocarcinoma. *Nat Med* 2016;**22**:278–87.
10. Andersen V, Christensen J, Ernst A, Jacobsen BA, Tjonneland A, Krarup HB, et al. Polymorphisms in NF-kappaB, PXR, LXR, PPARgamma and risk of inflammatory bowel disease. *World J Gastroenterol* 2011;**17**:197–206.

11. Oladimeji P, Cui H, Zhang C, Chen T. Regulation of PXR and CAR by protein−protein interaction and signaling crosstalk. *Expet Opin Drug Metabol Toxicol* 2016;**12**:997−1010.
12. Venkatesh M, Mukherjee S, Wang H, Li H, Sun K, Benechet AP, et al. Symbiotic bacterial metabolites regulate gastrointestinal barrier function *via* the xenobiotic sensor PXR and Toll-like receptor 4. *Immunity* 2014;**41**:296−310.
13. Poudel S, Huber AD, Chen T. Regulation of nuclear receptors PXR and CAR by small molecules and signal crosstalk: roles in drug metabolism and beyond. *Drug Metab Dispos* 2023;**51**:228−36.
14. Zhou J, Zhai Y, Mu Y, Gong H, Uppal H, Toma D, et al. A novel pregnane X receptor-mediated and sterol regulatory element-binding protein-independent lipogenic pathway. *J Biol Chem* 2006;**281**:15013−20.
15. Lehmann JM, McKee DD, Watson MA, Willson TM, Moore JT, Kliewer SA. The human orphan nuclear receptor PXR is activated by compounds that regulate CYP3A4 gene expression and cause drug interactions. *J Clin Invest* 1998;**102**:1016−23.
16. Wang J, Bwayi M, Gee RRF, Chen T. PXR-mediated idiosyncratic drug-induced liver injury: mechanistic insights and targeting approaches. *Expet Opin Drug Metabol Toxicol* 2020;**16**:711−22.
17. Komander D, Rape M. The ubiquitin code. *Annu Rev Biochem* 2012;**81**:203−29.
18. Zhou W, Slingerland JM. Links between oestrogen receptor activation and proteolysis: relevance to hormone-regulated cancer therapy. *Nat Rev Cancer* 2014;**14**:26−38.
19. Burns KA, Vanden Heuvel JP. Modulation of PPAR activity *via* phosphorylation. *Biochim Biophys Acta* 2007;**1771**:952−60.
20. Balaji V, Pokrzywa W, Hoppe T. Ubiquitylation pathways in insulin signaling and organismal homeostasis. *Bioessays* 2018;**40**:e1700223.
21. Escobar-Henriques M, Altin S, Brave FD. Interplay between the ubiquitin proteasome system and mitochondria for protein homeostasis. *Curr Issues Mol Biol* 2020;**35**:35−58.
22. Rana R, Coulter S, Kinyamu H, Goldstein JA. RBCK1, an E3 ubiquitin ligase, interacts with and ubiquitinates the human pregnane X receptor. *Drug Metab Dispos* 2013;**41**:398−405.
23. Ong SS, Goktug AN, Elias A, Wu J, Saunders D, Chen T. Stability of the human pregnane X receptor is regulated by E3 ligase UBR5 and serine/threonine kinase DYRK2. *Biochem J* 2014;**459**:193−203.
24. Qin M, Xin Y, Bian Y, Yang X, Xi T, Xiong J. Phosphorylation-induced ubiquitination and degradation of PXR through CDK2−TRIM21 axis. *Cells* 2022;**11**:264.
25. Lu Y, Li J, Cheng D, Parameswaran B, Zhang S, Jiang Z, et al. The F-box protein FBXO44 mediates BRCA1 ubiquitination and degradation. *J Biol Chem* 2012;**287**:41014−22.
26. Sjogren B, Swaney S, Neubig RR. FBXO44-mediated degradation of RGS2 protein uniquely depends on a cullin 4B/DDB1 complex. *PLoS One* 2015;**10**:e0123581.
27. Bwayi MN, Garcia-Maldonado E, Chai SC, Xie B, Chodankar S, Huber AD, et al. Molecular basis of crosstalk in nuclear receptors: heterodimerization between PXR and CAR and the implication in gene regulation. *Nucleic Acids Res* 2022;**50**:3254−75.
28. Lin W, Wu J, Dong H, Bouck D, Zeng FY, Chen T. Cyclin-dependent kinase 2 negatively regulates human pregnane X receptor-mediated *CYP3A4* gene expression in HepG2 liver carcinoma cells. *J Biol Chem* 2008;**283**:30650−7.
29. Huber AD, Li Y, Lin W, Galbraith AN, Mishra A, Porter SN, et al. SJPYT-195: a designed nuclear receptor degrader that functions as a molecular glue degrader of GSPT1. *ACS Med Chem Lett* 2022;**13**:1311−20.
30. Connelly JP, Pruett-Miller SM. CRIS.py: a versatile and high-throughput analysis program for CRISPR-based genome editing. *Sci Rep* 2019;**9**:4194.
31. Livak KJ, Schmittgen TD. Analysis of relative gene expression data using real-time quantitative PCR and the $2^{-\Delta\Delta CT}$ method. *Methods* 2001;**25**:402−8.
32. Dixon AS, Schwinn MK, Hall MP, Zimmerman K, Otto P, Lubben TH, et al. NanoLuc complementation reporter optimized for accurate measurement of protein interactions in cells. *ACS Chem Biol* 2016;**11**:400−8.
33. Schwinn MK, Machleidt T, Zimmerman K, Eggers CT, Dixon AS, Hurst R, et al. CRISPR-mediated tagging of endogenous proteins with a luminescent peptide. *ACS Chem Biol* 2018;**13**:467−74.
34. Lin W, Wang YM, Chai SC, Lv L, Zheng J, Wu J, et al. SPA70 is a potent antagonist of human pregnane X receptor. *Nat Commun* 2017;**8**:741.
35. Ghandi M, Huang FW, Jane-Valbuena J, Kryukov GV, Lo CC, McDonald 3rd ER, et al. Next-generation characterization of the cancer cell line encyclopedia. *Nature* 2019;**569**:503−8.
36. Shen JZ, Qiu Z, Wu Q, Finlay D, Garcia G, Sun D, et al. FBXO44 promotes DNA replication-coupled repetitive element silencing in cancer cells. *Cell* 2021;**184**:352−369.e23.
37. Nabet B, Roberts JM, Buckley DL, Paulk J, Dastjerdi S, Yang A, et al. The dTAG system for immediate and target-specific protein degradation. *Nat Chem Biol* 2018;**14**:431−41.
38. Petroski MD, Deshaies RJ. Function and regulation of cullin-RING ubiquitin ligases. *Nat Rev Mol Cell Biol* 2005;**6**:9−20.
39. Glenn KA, Nelson RF, Wen HM, Mallinger AJ, Paulson HL. Diversity in tissue expression, substrate binding, and SCF complex formation for a lectin family of ubiquitin ligases. *J Biol Chem* 2008;**283**:12717−29.
40. Li T, Chen W, Chiang JY. PXR induces CYP27A1 and regulates cholesterol metabolism in the intestine. *J Lipid Res* 2007;**48**:373−84.
41. Staudinger JL, Goodwin B, Jones SA, Hawkins-Brown D, MacKenzie KI, LaTour A, et al. The nuclear receptor PXR is a lithocholic acid sensor that protects against liver toxicity. *Proc Natl Acad Sci U S A* 2001;**98**:3369−74.
42. Xie W, Radominska-Pandya A, Shi Y, Simon CM, Nelson MC, Ong ES, et al. An essential role for nuclear receptors SXR/PXR in detoxification of cholestatic bile acids. *Proc Natl Acad Sci U S A* 2001;**98**:3375−80.
43. Kast HR, Goodwin B, Tarr PT, Jones SA, Anisfeld AM, Stoltz CM, et al. Regulation of multidrug resistance-associated protein 2 (ABCC2) by the nuclear receptors pregnane X receptor, farnesoid X-activated receptor, and constitutive androstane receptor. *J Biol Chem* 2002;**277**:2908−15.
44. Sugatani J, Nishitani S, Yamakawa K, Yoshinari K, Sueyoshi T, Negishi M, et al. Transcriptional regulation of human *UGT1A1* gene expression: activated glucocorticoid receptor enhances constitutive androstane receptor/pregnane X receptor-mediated UDP-glucuronosyltransferase 1A1 regulation with glucocorticoid receptor-interacting protein 1. *Mol Pharmacol* 2005;**67**:845−55.
45. Cai X, Young GM, Xie W. The xenobiotic receptors PXR and CAR in liver physiology, an update. *Biochim Biophys Acta, Mol Basis Dis* 2021;**1867**:166101.
46. di Masi A, De Marinis E, Ascenzi P, Marino M. Nuclear receptors CAR and PXR: molecular, functional, and biomedical aspects. *Mol Aspect Med* 2009;**30**:297−343.
47. Lamba V, Yasuda K, Lamba JK, Assem M, Davila J, Strom S, et al. PXR (NR1I2): splice variants in human tissues, including brain, and identification of neurosteroids and nicotine as PXR activators. *Toxicol Appl Pharmacol* 2004;**199**:251−65.
48. Dotzlaw H, Leygue E, Watson P, Murphy LC. The human orphan receptor PXR messenger RNA is expressed in both normal and neoplastic breast tissue. *Clin Cancer Res* 1999;**5**:2103−7.
49. Bauer B, Hartz AM, Fricker G, Miller DS. Pregnane X receptor up-regulation of P-glycoprotein expression and transport function at the blood−brain barrier. *Mol Pharmacol* 2004;**66**:413−9.
50. Ilyin GP, Serandour AL, Pigeon C, Rialland M, Glaise D, Guguen-Guillouzo C. A new subfamily of structurally related human F-box proteins. *Gene* 2002;**296**:11−20.
51. Ponten F, Gry M, Fagerberg L, Lundberg E, Asplund A, Berglund L, et al. A global view of protein expression in human cells, tissues, and organs. *Mol Syst Biol* 2009;**5**:337.
52. Miki Y, Suzuki T, Tazawa C, Blumberg B, Sasano H. Steroid and xenobiotic receptor (SXR), cytochrome P450 3A4 and multidrug

resistance gene 1 in human adults and fetal tissues. *Mol Cell Endocrinol* 2005;**231**:75−85.
53. Chrencik JE, Orans J, Moore LB, Xue Y, Peng L, Collins JL, et al. Structural disorder in the complex of human pregnane X receptor and the macrolide antibiotic rifampicin. *Mol Endocrinol* 2005;**19**:1125−34.
54. Wang Z, Liu P, Inuzuka H, Wei W. Roles of F-box proteins in cancer. *Nat Rev Cancer* 2014;**14**:233−47.
55. Skaar JR, Pagan JK, Pagano M. Mechanisms and function of substrate recruitment by F-box proteins. *Nat Rev Mol Cell Biol* 2013;**14**:369−81.
56. de Coo A, Cruz R, Quintela I, Herrera D, Sanz M, Diz P, et al. Genome-wide association study of stage III/IV grade C periodontitis (former aggressive periodontitis) in a Spanish population. *J Clin Periodontol* 2021;**48**:896−906.
57. Cao Q, Zhang S, Wang J, Wang Y, Pan C, Wang X, et al. Focal facial dermal dysplasias type III: two families with Setleis syndrome in China. *J Dermatol* 2022;**49**:1057−61.
58. Gu Y, Ma X, Li J, Ma Y, Zhang Y. Identification of candidate targets for the diagnosis and treatment of atherosclerosis by bioinformatics analysis. *Am J Transl Res* 2021;**13**:4137−51.
59. Li S, Yuan L, Xu ZY, Xu JL, Chen GP, Guan X, et al. Integrative proteomic characterization of adenocarcinoma of esophagogastric junction. *Nat Commun* 2023;**14**:778.
60. Sui Y, Park SH, Wang F, Zhou C. Perinatal bisphenol A exposure increases atherosclerosis in adult male PXR-humanized mice. *Endocrinology* 2018;**159**:1595−608.
61. Sui Y, Park SH, Helsley RN, Sunkara M, Gonzalez FJ, Morris AJ, et al. Bisphenol A increases atherosclerosis in pregnane X receptor-humanized ApoE deficient mice. *J Am Heart Assoc* 2014;**3**:e000492.
62. Sui Y, Meng Z, Park SH, Lu W, Livelo C, Chen Q, et al. Myeloid-specific deficiency of pregnane X receptor decreases atherosclerosis in LDL receptor-deficient mice. *J Lipid Res* 2020;**61**:696−706.
63. Sun L, Sun Z, Wang Q, Zhang Y, Jia Z. Role of nuclear receptor PXR in immune cells and inflammatory diseases. *Front Immunol* 2022;**13**:969399.
64. Chen Y, Tang Y, Wang MT, Zeng S, Nie D. Human pregnane X receptor and resistance to chemotherapy in prostate cancer. *Cancer Res* 2007;**67**:10361−7.
65. Chen Y, Tang Y, Chen S, Nie D. Regulation of drug resistance by human pregnane X receptor in breast cancer. *Cancer Biol Ther* 2009;**8**:1265−72.